12th International Symposium on Turbulence and Shear Flow Phenomena (TSFP12)
Osaka, Japan, July 19–22, 2022

THE NEAR-WAKE OF DISCRETE ROUGHNESS ELEMENTS ON SWEPT WINGS: TOMOGRAPHIC PTV MEASUREMENTS

Giulia Zoppini
AWEP Department-Aerodynamics
Delft University of Technology
The Netherlands, 2629HS
g.zoppini@tudelft.nl

Theodoros Michelis
AWEP Department-Aerodynamics
Delft University of Technology
The Netherlands, 2629HS
t.michelis@tudelft.nl

Daniele Ragni
AWEP Department-Wind Energy-Aeroacoustics
Delft University of Technology
The Netherlands, 2629HS
d.ragni@tudelft.nl

Marios Kotsonis
AWEP Department-Aerodynamics
Delft University of Technology
The Netherlands, 2629HS
m.kotsonis@tudelft.nl

ABSTRACT

This work presents the first reported experimental characterization of the flow field in the direct vicinity of discrete roughness elements (DRE), in a swept wing boundary layer. High magnification tomographic Particle Tracking Velocimetry (3D-PTV) measurements are used to acquire time-averaged velocity and standard deviation fields in a 3D volume directly aft of the DRE elements. The collected data detail the near-element flow topology, providing information on the developing wake and emerging flow structures, their organization and amplitude evolution. A transient growth behaviour is identified in the element wake, while onset and growth of crossflow instabilities is observed further downstream. As such, the near element flow is confirmed to be a fundamental part of the receptivity process, contributing in setting the initial amplitudes for the crossflow instability evolution.

INTRODUCTION

Laminar to turbulent transition of swept wing boundary layers (BL) in low freestream turbulence environments, is dominated by the development of stationary crossflow instabilities (CFI, Bippes, 1999; Wassermann & Kloker, 2002; Saric *et al.*, 2003; Serpieri & Kotsonis, 2016). One of the most challenging and least described phases of the CFI development, is receptivity (Mack, 1984), defined as the process through which the external disturbances (mainly freestream turbulence and surface roughness) enter the boundary layer leading to the onset of instabilities. Previous investigations, proved that the stationary CFI are mostly affected by surface roughness (Saric *et al.*, 2003; Downs & White, 2013). This sensitivity is typically profited towards obtaining a more uniform flow field dominated by a monochromatic crossflow mode. Specifically, discrete roughness elements (DRE) can be arranged in a periodic array along the wing span with a fixed element spacing corresponding to the desired mode wavelength (Reibert *et al.*, 1996; Saric *et al.*, 1998; Serpieri & Kotsonis, 2016). The use of DREs to condition experimental or numerical CFI configurations is well established, albeit governed by a little-understood receptivity process. However, of the numerous studies dedicated to stationary CFI adopting this technique, only few numerical simulations focussed on the investigation of the near-element flow features and the receptivity process (Brynjell-Rahkola *et al.*, 2015; Kurz & Kloker, 2016). This relates to the limited experimental access to the small region of interest, as well as to the numerous parameters involved in the relation between the external disturbances and CFI onset.

The numerical simulations conducted by Brynjell-Rahkola *et al.* (2015) and Kurz & Kloker (2016), identified the development of a horseshoe vortex system around and aft of the element, in analogy with 2D-BL flows (Baker, 1979). A low-speed streak develops in the elements' wake, surrounded by two adjacent high-speed streaks. The presence of the crossflow velocity component in the baseflow, introduces a significant asymmetry in the flow features, leading to a flow field dominated by the crossflow direction of rotation. Accordingly, all the structures co-rotating with the crossflow are sustained in their downstream evolution, while the counter rotating structures are dampened. The discussed DNS studies, provide significant insights regarding the near-DRE flow topology and the instabilities development, however they still lack a full characterization of the receptivity process relating the external forcing to the CFI onset. Additionally, numerous experimental and numerical works investigating roughness elements in 2D-BL flows, identified transient mechanisms as fundamental for the near-wake development (White *et al.*, 2005; Breuer & Kuraishi, 1994; Cherubini *et al.*, 2013). Therefore, the initial growth of transient near-wake instabilities is a fundamental part of the receptivity process, eventually setting the onset amplitudes for the modal CFI.

The present work provides the first experimental investigation of the near-DRE flow field, aiming at further clarifying the receptivity process and the flow features dominating the CFI onset. The measurements are conducted through specialized high-magnification tomographic particle tracking velocimetry (PTV), acquiring 3D velocity fields in the element vicinity, while modifying the DRE height. The collected experimental data, provide a characterization of the near-element flow topology, identifying the dominant flow structures and their organization. The structures downstream evolution is

analysed estimating the instabilities amplitudes and spectral composition, allowing for the identification of transient mechanisms occurring in the element near-wake.

METHODOLOGY

Wind Tunnel, Swept Wing Model and DREs

The presented measurements are performed on an in-house designed swept wing model (M3J), with constant chord c=1273mm and sweep angle 45° (Serpieri, 2018). The wing model features a favourable pressure gradient up to x/c=0.63, thus allowing investigation of primary and secondary CFI and BL transition (Serpieri & Kotsonis, 2016).

The measurements are performed in the low speed low turbulence wind tunnel, an atmospheric closed return tunnel at the TU Delft, featuring low freestream turbulence level in the test section flow (Serpieri, 2018). The flow fields are acquired at a fixed angle of attack (α=-3.36°) and freestream Reynolds number (Re_c=2.17×10^6). The reference system used in this investigation (x,y,z and corresponding velocities *u,v,w*) has its x and z axes orthogonal and aligned to the leading edge, respectively.

Following Reibert *et al.* (1996), DRE arrays are applied on the wing in order to focus the developing CFI on a single monochromatic mode. The forced mode is chosen to coincide with the most critical wavelength λ_1=8mm for the present conditions, as indicated by previous investigations and linear stability simulations (LST, Malik *et al.*, 1999; Serpieri, 2018). The array elements have a cylindrical shape with nominal diameter d$\simeq$2mm. To gain better access to the experimental domain of interest, DREs are applied at a fixed chord location of x/c=0.15 (Zoppini *et al.*, 2022). Three different element heights are considered throughout this work, k_1=0.1mm, k_2=0.2mm and k_3=0.3mm, corresponding to roughness Reynolds numbers of Re_{k_1}=25, Re_{k_2}=90 and Re_{k_3}=190 ($Re_k = \frac{k \times |\mathbf{u}(k)|}{\nu}$, Gregory & Walker, 1956).

Tomographic PTV

The instantaneous velocity distribution is measured through a tomographic velocimetry configuration (Elsinga *et al.*, 2006) in a 3D domain centred at x/c=0.165 and extending for 35×3.5×35mm along x,y,z. The three directions are non-dimensionalized by the chord, $\overline{\delta}_{99}$ (i.e. the δ_{99} of the laminar boundary layer at x/c=0.15) and λ_1 respectively.

The light source is a Quantel Evergreen Nd:YAG dual cavity laser (200 mJ pulse energy), optically accessing the test section through a plexiglass window. Through suitable optics, the laser beam is shaped in a 4mm thick sheet parallel to the wing surface in the area of interest. The flow is imaged through 4 sCMOS LaVision Imager cameras equipped with a 2X teleconverter, a 200mm lens and a lens-tilt mechanism to comply with the Scheimpflug condition. This optical arrangement results in a 400mm focal length for each camera, with $f_{\#}$=11 in order to keep the particles in focus throughout the entire volume depth. The cameras are installed on the outer side of the test section with a tomographic aperture of approximately 45°. The model surface is at $\simeq$1m distance, resulting in a resolution of 67px/mm. Flow seeding is obtained by dispersing 0.5μm droplets of a water-glycol mixture in the wind tunnel.

For each considered case, 4000 image pairs are acquired at a frequency of 15Hz. The time interval between paired images is 8μs, corresponding to a freestream particle displacement of almost 10 pixels. Each image pair is processed in LaVision DaVis 10 through a 2-pulse shake-the-box algorithm (Wieneke, 2012) to identify the particle trajectories in the acquired 3D volume. Binning and conversion to a Cartesian grid of the obtained particle tracks, are performed through an in-house developed Matlab routine. The final vector spacing is approximately 0.25mm in the xz plane, and 0.04mm along y.

Time-averaged ($\overline{u},\overline{v},\overline{w}$) and standard deviation (u',v',w') velocity fields are obtained for all three velocity components in the x,y,z domain. For the sake of brevity, the main data processing techniques adopted in this work, are briefly described hereafter as only applied to $\overline{u}$. The treatment of $\overline{v}$ and $\overline{w}$ follow a similar procedure. The wall-normal BL evolution ($\overline{u}_b$) is estimated by averaging the $\overline{u}$ velocity signal along z for each fixed xy location acquired (i.e. $\overline{u}_b$). The freestream velocity $\overline{u}_\infty$ is estimated as the average of $\overline{u}_b$ for $y > \delta_{99}$. The disturbance velocity field ($\overline{u}_d$) can be computed as $\overline{u}_d = \overline{u}(x,y,z) - \overline{u}_b(x,y)$. An estimation of the wall-normal evolution of the perturbations in the boundary layer is then obtained by computing $\langle u \rangle_z$, i.e. the root mean square (rms) of the $\overline{u}_d$ velocity signal along z for each fixed x,y-location (Reibert *et al.*, 1996; Tempelmann *et al.*, 2012). Furthermore, a spatial Fourier analysis is performed on the spanwise velocity signal at each x,y-location ($\mathrm{FFT}_z(\overline{u})$), in order to characterize the development of the dominant crossflow mode and its harmonics. Finally, the total perturbation amplitude as well as the individual Fourier modes amplitudes are estimated by respectively integrating the $\langle \overline{u} \rangle_z$ profile or the corresponding Fourier shape function along y, following the integral amplitude definition by Downs & White (2013); Reibert *et al.* (1996). This provides an estimation of the modes growth and evolution along the airfoil chord, along with information on the CFI onset amplitude.

RESULTS DISCUSSION

The investigation of the time-averaged velocity fields, allows for the direct characterization of the near-element flow topology and of the stationary perturbations. Figure 1 shows the $\overline{u}_d$ (figures (a-c)), and u' contours (figures (d-f)) for a BL forced with Re_{k_3}. Both the xz and yz planes reported in figures 1(a-c), indicate that a low-speed streak develops aft of each cylindrical element, in correspondence to the element's wake. The low-speed wake is accompanied by two high speed streaks developing on its sides. The latter correspond well to the horseshoe vortex legs wrapping around and extending aft of the elements, which induce a momentum redistribution process leading to the streak formation (Kurz & Kloker, 2016; Baker, 1979). In between the elements, the flow maintains a laminar behaviour, as the introduced perturbations are relatively weak in amplitude. This is confirmed by the velocity contours in the yz plane extracted at x_1=0.154c (figure 1(b)), which show that the developing streaks structures only affect the near-wall BL region (i.e. up to y$\simeq 0.5\delta_{99}$), without introducing the boundary layer velocity modulation typical of CFI.

The developing flow topology closely resembles the near-wake flow features incurred by isolated roughness elements in 2D or 3D-BL (e.g. Brynjell-Rahkola *et al.*, 2015; Kurz & Kloker, 2016; Baker, 1979; Loiseau *et al.*, 2014). The main difference between the flow features pertaining to the two BL is linked to the overall flow asymmetry introduced by the presence of the crossflow velocity component in the baseflow. This is clearly visible in the presented results, as the high speed streaks developing on the two sides of the wake, undergo a different growth and evolution process. In particular, in figure 1(a) the outboard high-speed streak (full line) is decaying being substituted by an outer low-speed streak (dash-dot line); while the inboard high-speed streak (dashed line) per-

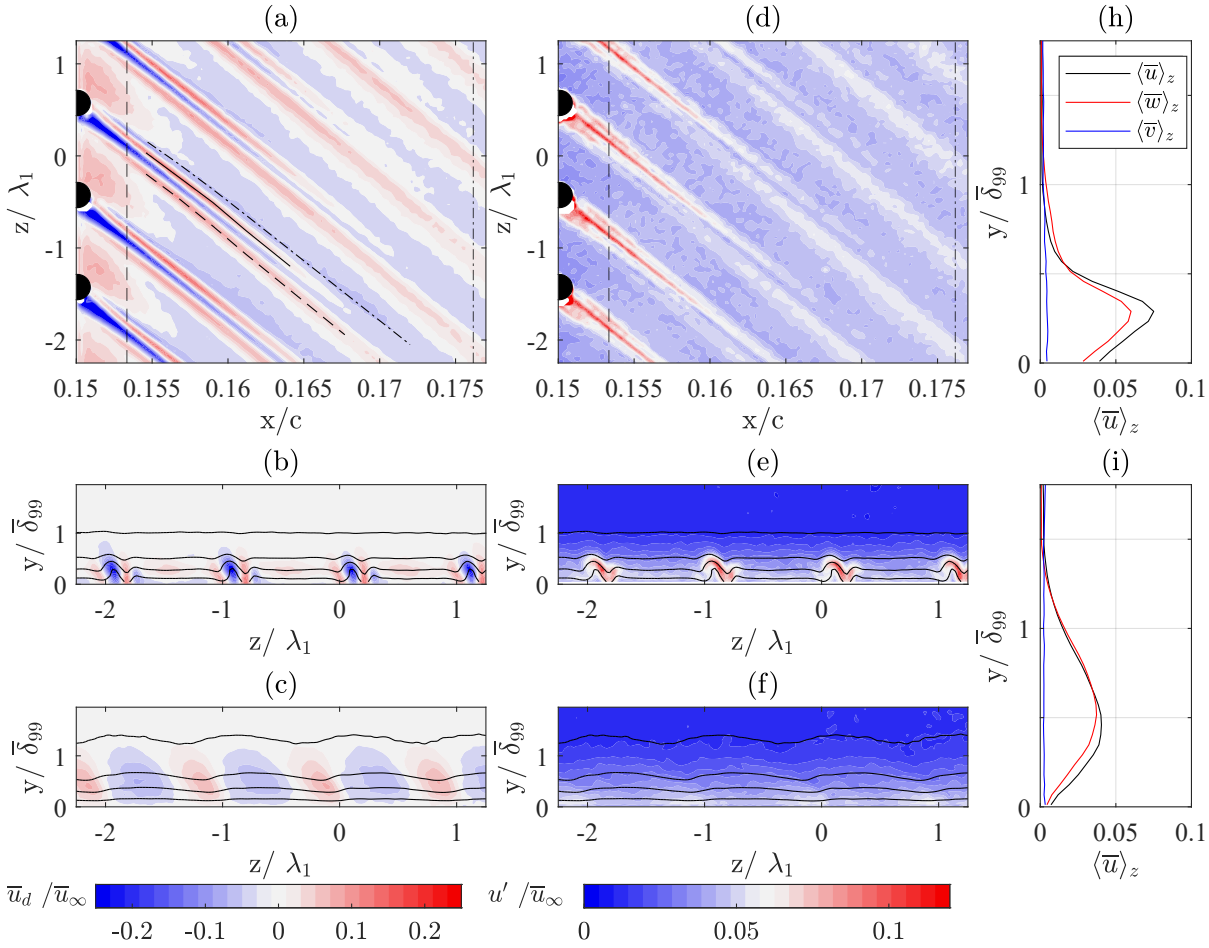

Figure 1. Contours of (a-c) $\overline{u}_d$ and (d-f) u' for Re_{k_3}=192 forcing. Time-averaged $\overline{u}_d$ fields (a, d) in the xz plane at y=0.17$\overline{\delta}_{99}$; (b, e) in the yz plane at x_1=0.154c (vertical dashed line in (a)), and (c, f) at x_2=0.176c (vertical dash-dot line). (h, i) Velocity disturbance profiles $\langle\overline{u}\rangle_z$ at x_1 and x_2 for all three velocity components.

sists in the flow, with lowered amplitudes, up to the end of the acquired domain. As a result, the far-wake flow evolution is dominated by a simple high- and low-speed region alternation, given by the downstream development of the inboard high-speed streak and the outer low-speed streak respectively. This is confirmed by the velocity contours collected in the downstream yz plane (x_2=0.176c, figure 1(c)), showing that the disturbances are affecting the whole boundary layer wall-normal extent, thus modulating the baseflow. The spanwise modulation of the BL velocity and momentum visible in figure 1(c), is a typical feature of CFI development (Bippes, 1999; Saric *et al.*, 2003) . Nonetheless, the identified flow features describe a BL only weakly affected by CFI, as the acquired flow domain is only representative for the CFI initial growth stages mostly unaffected by non-linearities. Finally, all the observed streak structures appear to be developing at an angle of almost 6° with respect to the freestream direction. This value is comparable to the angle predicted by LST as well as to the angle measured between the developing crossflow vortices and the freestream velocity in the same set-up at more downstream chord locations (Serpieri & Kotsonis, 2016).

The u' contours (figures 1(d-f)) reflect the stationary streak organization and development described above. More specifically, in the element vicinity, stronger velocity fluctuations are localized in correspondence of the low-speed streak, slightly shifting towards the region between the outboard high- and low-speed streaks as moving downstream. This is once again in agreement with studies dedicated to isolated roughness elements, suggesting that the developing near-wake instabilities are strongly related to the shear layers characterizing the near-wake flow region (figure 1(e), Brynjell-Rahkola *et al.*, 2015; Klebanoff *et al.*, 1992). Overall, the fluctuations level reduces as the flow evolves downstream and localizes in correspondence of the inboard high-speed streak. This is accompanied by the growth of the instability structures size along the y direction (figures 1(h-i)), which is also connected to the natural thickening of the BL.

To further characterize the observed flow features, a spatial Fourier analysis of the span-wise $\overline{u}_d$ velocity signal is performed. Figure 2(a) shows the spectra development in the x-λ_z plane extracted at y/$\overline{\delta}^*$=0.17. The forced λ_1 mode is clearly present in the flow field corresponding to a significant spectral energy peak. However, in the near-wake region (i.e. at x_1), the λ_1 mode development is accompanied by strong harmonics content. This effect can be associated to the pseudo-pulse behaviour of the DRE wake, which contains all spatial frequencies due to its highly localised form. The observed modes, however, are not necessarily instability modes, as it is the finite diameter of the DRE that is responsible for the observed energy distribution. In particular, up to 51% of the total perturbation spectral energy is contained by the dominant mode and its first four harmonics, confirming these modes absorb the majority of the flow energy. At the most downstream location considered (x_2=0.176c), the spectra peaks reach overall lower

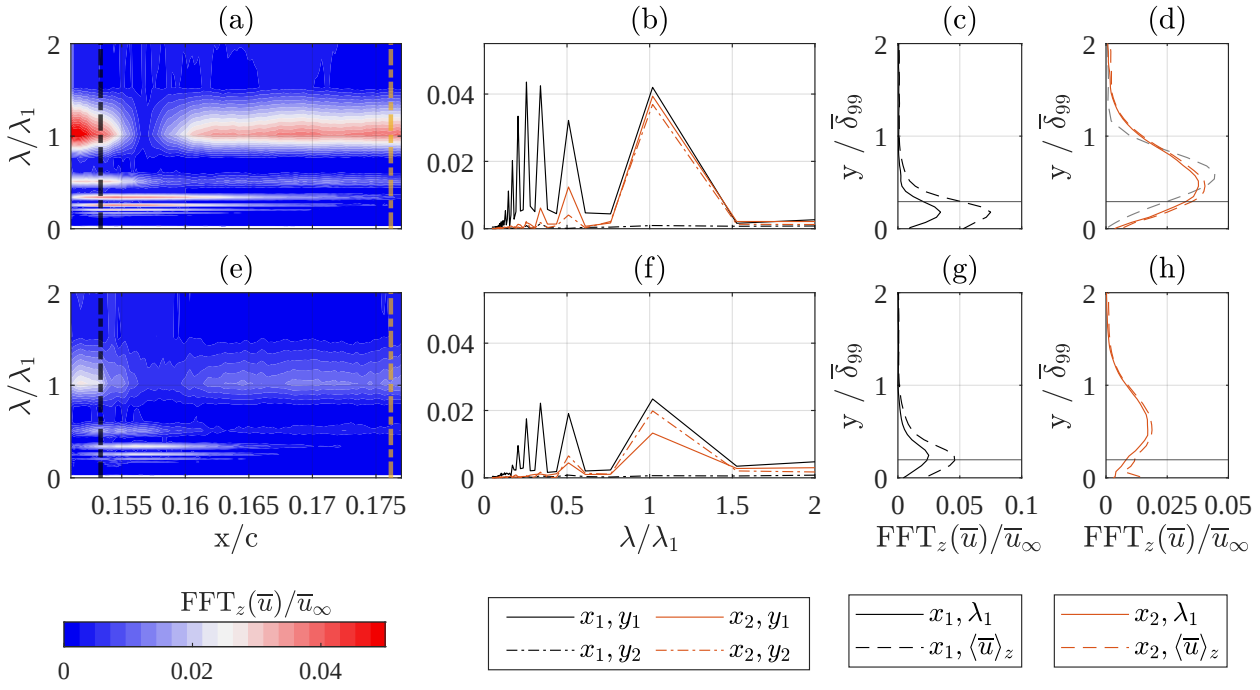

Figure 2. Spanwise Fourier analysis of $\overline{u}_d$ for forcing at (a-d) Re_{k_3} and (e-h) Re_{k_2}. (a, e) Spectra in the x-λ_z plane. (b, f) Spectra extracted at fixed x and y with x_1=0.154c; x_2=0.176c; y_1=0.17$\overline{\delta}_{99}$; y_2=0.6$\overline{\delta}_{99}$. (c, g) $\langle\overline{u}\rangle_z$ profile and λ_1 shape function at x_1 and (d, h) at x_2. LST λ_1 shape function (gray - - profile), element height (horizontal full line).

amplitude values, and the λ_1 mode is now evidently dominating the flow evolution only accompanied by weak λ_2 and λ_3 harmonics (figure 2(b)). This aspect can be further investigated by comparing the λ_1 mode shape functions extracted from the Fourier analysis with the $\langle\overline{u}\rangle_z$ profile for the two considered chord locations, as shown in figure 2(c). At x_1, the two profiles show a comparable shape, however their maximum amplitude significantly differs. This can be related to the high energy contained in the harmonic modes, which contribute to the near-wake flow perturbations development. On the other hand, at x_2 where the λ_1 mode dominates the flow development, the corresponding shape functions satisfactorily describe the total flow perturbation. The spectra reported as dash-dot lines in figure 2(b) are extracted at a higher wall-distance ($y/\overline{\delta}^*$=0.6). At this y location, the near-wake spectra extracted at x_1 shows no relevant modal content. This is in agreement with figure 1(c, d), as the upper half of the boundary layer is still mostly unaffected by flow perturbations in this flow region. Instead, at x_2, the spectra extracted at the two wall-normal locations (figure 1(b)) display comparable features, with the dominant peak corresponding to mode λ_1 accompanied by weaker harmonics. A similar analysis is reported for the Re_{k_2} case (figures 2(d-f)), showing comparable flow characteristics, despite the overall smaller amplitudes and spectral energy of the developing instabilities.

From the $\overline{u}_d$ and u' analysis of figure 1, an initial growth phase can be identified for both the high- and low-speed streaks amplitudes in the near-wake region. More specifically, figure 3(a) quantifies the chordwise evolution of the high-/low-speed streak amplitudes (A_{str}) computed as maximum/minimum value of the $\overline{u}_d$ velocity field respectively. The amplitude trends extracted for Re_{k_2} and Re_{k_3} forcing, show a mild growth of the high-speed structures in the near-wake region, followed by an amplitude decay shortly downstream. The low-speed structures absolute amplitude is instead monotonically decaying as evolving downstream. Comparable behaviour is expected for the Re_{k_1} forcing case, however is it hindered by the overall weaker instabilities. Thus, this case is disregarded in the following analysis. A relative streak amplitude metric is as well computed, following the definition given by Andersson *et al.* (2001), i.e. A_{And}=0.5*(max($\overline{u}_d$) - min($\overline{u}_d$)). The resulting amplitude trends are reported in figure 3(b), and confirm that mild instability growth occurs in the near-wake, followed by an amplitude decay. Additionally, none of the considered cases reaches an amplitude value higher than the critical threshold identified by Andersson *et al.* (2001) for the laminar structure breakdown (i.e. A_{And}=0.2$\overline{u}_\infty$).

The observed initial instability growth is further investigated by analysing the integral total perturbation amplitude and the individual Fourier modes amplitude, estimated following the definition given by Downs & White (2013). The resulting trends are reported in figure 4 for Re_{k_3} and Re_{k_2}, showing comparable flow features. Apart from the initial amplitude decay, the total perturbation amplitude shows little chordwise variations within the acquired domain. Nonetheless, the modal amplitude associated to λ_1 significantly decays immediately aft of the element. The λ_1 mode recovers amplitude values comparable to the total perturbation further downstream (i.e. downstream of x/c=0.165), indicating that it dominates the BL evolution in this flow region. The second harmonic λ_2 follows a comparable trend, retaining lower amplitude values up to the domain end. However, the higher harmonics (λ_3-λ_6) all show a mild amplitude growth in the element vicinity, sustaining the total perturbation amplitude. These modes all decay shortly downstream, leaving a boundary layer dominated by the primary stationary mode. The spectral energy distribution among individual Fourier modes closely resembles the observations by White *et al.* (2005), and suggests that a transient mechanism (possibly transient growth, Schmid & Henningson, 2001) driven by the stationary mode harmonics dominates

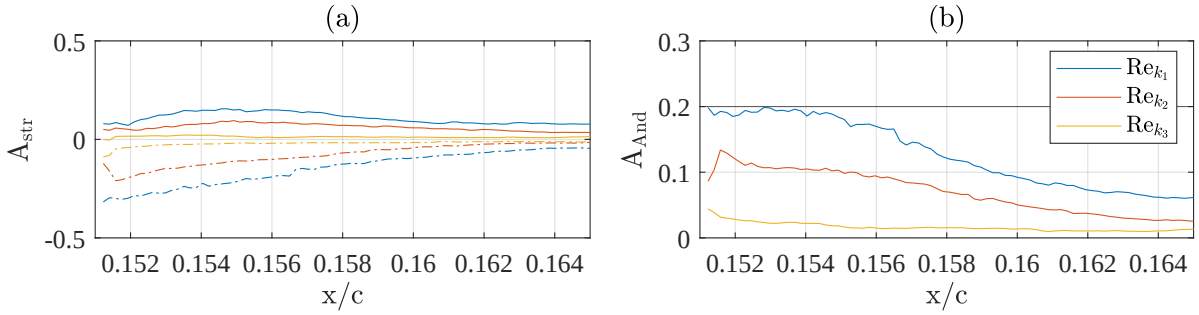

Figure 3. Amplitude analysis for varying Re_k (i.e. DRE amplitude). (a) Streak amplitude A_{str} for high-speed (full line) and low-speed (-. lines) streaks; (b) Andersson amplitudes A_{And} and amplitude limit for laminar streak breakdown (-. line) (Andersson *et al.*, 2001).

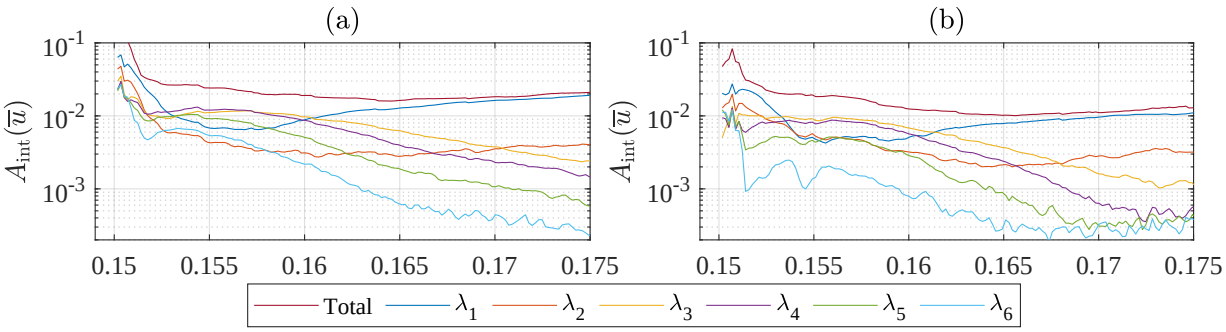

Figure 4. A_{int} for the total disturbance field and for the $\lambda_1 - \lambda_6$ Fourier harmonics for forcing cases (a) Re_{k_3} and (b) Re_{k_2}.

the near-wake flow evolution. Despite its short chordwise extent, a non-modal growth mechanism can lead to rapid initial growth of the near-wake instabilities, enhancing their downstream development. Eventually, such transient process contributes to setting the onset conditions for the CFI (Breuer & Kuraishi, 1994; Lucas, 2014), becoming a fundamental step in receptivity.

Based on the previous considerations, the onset of modal CFI would occur downstream of the transient process identified in the near-wake flow region. Following this hypothesis, the CFI onset amplitude A_0 can be estimated as the amplitude achieved by the λ_1 mode at x/c$\simeq$0.164 (i.e. $\simeq$9.5d downstream of the elements). Figure 5(a) shows the total perturbation amplitude A_{int} reaches a minimum value around x/c$\simeq$0.164, modally growing further downstream. In fact, the primary stationary mode contains almost 80% of the total perturbation energy at this chord location, dominating the BL evolution. Accordingly, the A_0 estimation delivers a representative value for the CFI onset amplitude corresponding to $A_0 \simeq 0.024\overline{u}_\infty$ for Re_{k_3}, $A_0 \simeq 0.012\overline{u}_\infty$ for Re_{k_2}. Using the extracted A_0 value, an effective N-factor (Saric *et al.*, 2019) can be computed from experimental data as $N_{eff}=\log(A_{int}/A_0)$, describing the CFI modal evolution downstream of x/c=0.164. The resulting growth curves are reported in figure 5(b) compared to the effective N-factor extracted for the λ_1 mode from the LST (N_{LST} Serpieri, 2018). The experimental growth trends and the numerical solution show a satisfactory match, confirming the exponential (i.e. modal) growth process followed by the instabilities downstream of x/c=0.164.

CONCLUSION

The near-element flow of roughness elements applied in a swept wing boundary layer, is experimentally investigated through high-magnification tomographic PTV. The flow field is forced by applying critically spaced DRE arrays at x/c=0.15 for various forcing amplitudes. Time-averaged and standard deviation velocity fields are acquired in a 3D volume located immediately downstream of the DRE.

The near-element stationary flow topology is dominated by a low-speed streak located in correspondence of the element wake, while two high-speed streaks develop on its sides. The presence of the crossflow velocity component in the baseflow induces a 6° misalignment between the freestream velocity vector and the developing streaks. Additionally, the flow field evolution is dominated by the crossflow-direction of rotation, resulting in an asymmetric downstream development of the identified flow structures. These effects lead to the formation of high- and low-speed regions alternating along the span in the downstream portion of the acquired domain. Their presence results in the modulation of the BL velocity and momentum, typically associated to the presence of CFI. However, the CFI onset occurs at a finite distance from the DRE location, suggesting that the development of the individual element wake is fundamental to set the flow conditions for the modal instabilities onset. This consideration is confirmed by the amplitude analysis, which indicates the presence of a transient mechanism dominating the near-wake evolution. In particular, the individual Fourier modes behaviour, shows that the primary mode and its second harmonics both decay in the element vicinity, while the higher harmonics initially grow sustaining the total perturbation amplitude. Further analysis is needed to fully characterize the observed transient mechanism. Nonetheless, by comparing the evolution of the total perturbation amplitude and of the individual λ_1 mode, a direct estimation of the CFI onset amplitude (A_0) is performed. The comparison of experimental and numerical growth rates based on A_0, confirms the exponential nature of the instabilities growth process

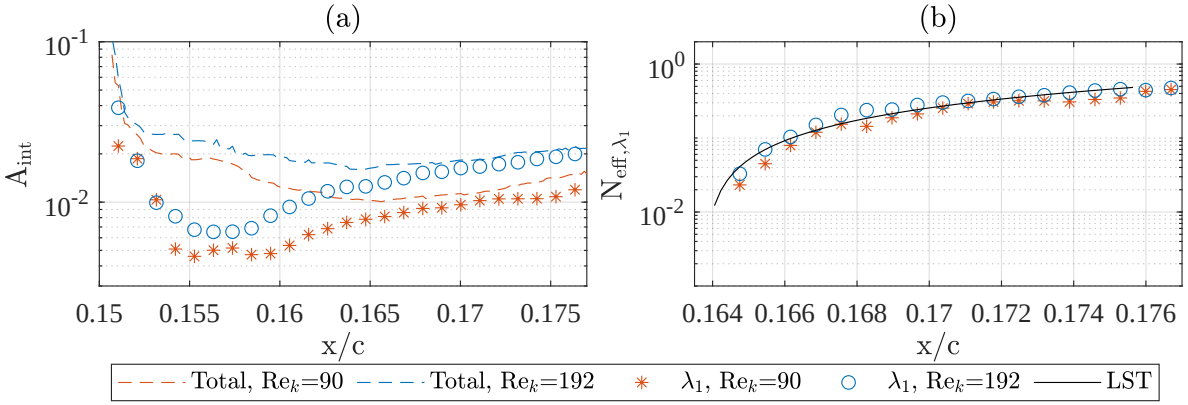

Figure 5. Experimental (a) A_{int} and (b) N_{eff} estimation for the λ_1 mode (symbols, 1 out of 5) and for the total perturbation amplitude (dashed line). N_{LST} estimation for the λ_1 mode (solid lines).

further downstream. Therefore, the transient instabilities identified in the element near-wake are confirmed to be a fundamental part of the receptivity process, contributing in setting the initial amplitudes for the modal CFI onset and downstream evolution.

REFERENCES

Andersson, P., Brandt, L., Bottaro, A. & Henningson, D.s. 2001 On the breakdown of boundary layer streaks. *Journal of Fluid Mechanics* **428**, 29–60.

Baker, CJ 1979 The laminar horseshoe vortex. *Journal of fluid mechanics* **95** (2), 347–367.

Bippes, H. 1999 Basic experiments on transition in three-dimensional boundary layers dominated by crossflow instability. *Progress in Aerospace Sciences* (35), 363–412.

Breuer, Kenneth S. & Kuraishi, Takeo 1994 Transient growth in two- and three-dimensional boundary layers. *Physics of Fluids* **6** (6), 1983–1993.

Brynjell-Rahkola, M., Schlatter, P., Hanifi, A. & Henningson, D.S. 2015 Global stability analysis of a roughness wake in a falkner-skan-cooke boundary layer. *Procedia IUTAM* **14**, 192–200.

Cherubini, Stefania, de Tullio, Marco, de Palma, Pietro & Pascazio, Giuseppe 2013 Transient growth in the flow past a three-dimensional smooth roughness element .

Downs, R.S. & White, E.B. 2013 Free-stream turbulence and the development of cross-flow disturbances. *Journal of Fluid Mechanics* **735**, 347–380.

Elsinga, G. E., Scarano, F., Wieneke, B. & van Oudheusden, B. W. 2006 Tomographic particle image velocimetry. *Experiments in Fluids* **41** (6), 933–947.

Gregory, N.T. & Walker, W.S. 1956 *The effect on transition of isolated surface excrescences in the boundary layer*. HM Stationery Office.

Klebanoff, P. S., Cleveland, W. G. & Tidstrom, K. D. 1992 On the evolution of a turbulent boundary layer induced by a three-dimensional roughness element. *Journal of Fluid Mechanics* **237**, 101–187.

Kurz, H.B.E. & Kloker, M.J. 2016 Mechanisms of flow tripping by discrete roughness elements in a swept-wing boundary layer. *Journal of Fluid Mechanics* **796**, 158–194.

Loiseau, J.C., Robinet, J.C., Cherubini, S. & Leriche, E. 2014 Investigation of the roughness-induced transition: global stability analyses and direct numerical simulations. *Journal of Fluid Mechanics* **760**, 175–211.

Lucas, J.M. 2014 Spatial optimal perturbations for transient growth analysis in three-dimensional boundary layers. PhD thesis.

Mack, L.M. 1984 Boundary-layer linear stability theory. *Tech. Rep.*. California Inst of Tech Pasadena Jet Propulsion Lab.

Malik, M.R., Li, F., Choudari, M.M. & Chang, C.L. 1999 Secondary instability of crossflow vortices and swept-wing boundary-layer transition. *Journal of Fluid Mechanics* **399**, 85–115.

Reibert, M., Saric, W.S., Carrillo, Jr.R. & Chapman, K. 1996 Experiments in nonlinear saturation of stationary crossflow vortices in a swept-wing boundary layer. In *34th Aerospace Sciences Meeting and Exhibit*. American Institute of Aeronautics and Astronautics.

Saric, W.S., Carrillo, R. & Reibert, M. 1998 Leading-edge roughness as a transition control mechanism.

Saric, W.S., Reed, H.L. & White, E.B. 2003 Stability and transition of three dimensional boundary layers. *Annual Review of Fluid Mechanics* **35** (1), 413–440.

Saric, W.S., West, D.E., Tufts, M.W. & Reed, H.L. 2019 Experiments on discrete roughness element technology for swept-wing laminar flow control. *AIAA Journal* **57** (2), 641–654.

Schmid, P.J. & Henningson, D.S. 2001 Applied mathematical sciences.

Serpieri, J. 2018 Cross-flow instability. PhD thesis.

Serpieri, J. & Kotsonis, M. 2016 Three-dimensional organisation of primary and secondary crossflow instability. *Journal of Fluid Mechanics* **799**, 200–245.

Tempelmann, D., Schrader, L.U., Hanifi, A., Brandt, L. & Henningson, D.S. 2012 Swept wing boundary-layer receptivity to localized surface roughness. *Journal of Fluid Mechanics* **711**, 516–544.

Wassermann, P. & Kloker, M. 2002 Mechanisms and passive control of crossflow-vortex-induced transition in a three-dimensional boundary layer. *Journal of Fluid Mechanics* **456**, 49–84.

White, Edward B., Rice, Justin M. & Ergin, F. Gökhan 2005 Receptivity of stationary transient disturbances to surface roughness. *Physics of Fluids* **17** (6), 064109.

Wieneke, Bernhard 2012 Iterative reconstruction of volumetric particle distribution. *Measurement Science and Technology* **24** (2).

Zoppini, G., Westerbeek, S., Ragni, D. & Kotsonis, M. 2022 Receptivity of crossflow instability to discrete roughness amplitude and location. *Journal of Fluid Mechanics* **939**.